Sorption Phenomena In Transient Vapor Intrusion Scenarios

Jonathan G. V. Ström[a], Shuai Xie[a], Eric M. Suuberg[a]

These authors contributed equally to this work

[a]*Brown University, School of Engineering, Providence, RI, USA*

Abstract

Abstract here

Keywords: Vapor intrusion, Temporal variability, Sorption, Attenuation factor

1. Introduction

Many vapor intrusion (VI) contaminants has the capacity to sorb onto soil and various common indoor materials, but the role and more importantly, the consequences of these sorption processes in VI are poorly understood[1, 2, 3]. The migration of contaminant vapors from its source into the VI affected building and potential indoor sources are usually the prime concern in VI investigations. Rarely is the sorbed contaminant vapors in the soil or indoor considered in an investigation, but these may potentially act as a capacitor, storing and releasing contaminant vapors in response to a change in contaminant concentration. Consequently, contaminant vapors may be much more persistent at a site that has undergone remediation, potentially reducing the effectiveness of mitigation systems, or impeding site investigations.

It is well recognized that building materials has the capacity that sorb pollutants. The sorptive capacity of various volatile organic compounds (VOCs) of concern in VI have been tested on a variety of building materials, such as density board[4], gypsum wallboard[5], and plywood and carpets[6]. However, most of these studies used relative high contaminant concentrations, usually around mg/m^3[4] or even higher. This is several magnitudes higher than the concentrations relevant in VI and due to the non-linear nature of sorption with respect to concentration, sorption studies at lower concentration are needed.

Preprint submitted to Building and Environment *November 22, 2019*

Email addresses: eric_suuberg@brown.edu (Eric M. Suuberg)

Most of the VOC sorption studies have also focused on the interaction between building materials and formaldehyde[5], toluene, and decane[6]. However, one of the contaminants of greatest concern in VI - trichloroethylene (TCE), has not received likewise attention. This is despite the fact that sorbing TCE (and other VOCs) on activated carbon is extensively used to treat indoor air contaminant and their use with passive sorption tube samplers[7].

Over the years many VI sites have been investigated for their potential exposure risk. Most of these are conducted by private industries but a few notable academic ventures exist as well. Two well-known examples of these are the studies of "Sun Devil Manor" near Hill Air Force Base in Utah, and a building in Indianapolis, Indiana. Both of these sites were outfitted with a wide variety of instrumentation to investigate the VI drivers at these sites. These studies yielded some of the richest VI datasets available and gave invaluable insights, in particular in the application of CPM[8] and sub-slab depressurization (SSD) mitigation systems[9, 10]. However, neither of these studies considered the role of sorption had at these sites.

The potential impact of sorption may perhaps be most significant in the application of the controlled pressure method and various mitigation schemes. The controlled pressure method (CPM) is the forced over- and depressurization of a building to max- and minimize the contaminant entry to the building. This aids the investigator to ascertain the worst-case VI scenario and help identify potential indoor contaminant sources[11, 8]. However, if the building has a large capacity to sorb contaminant vapors onto various materials, these may be sorbed and desorbed in response to the changing condition, potentially preventing corresponding changes in indoor air contaminant concentrations. The same is true for various mitigation schemes, while they may successfully prevent contaminant vapors from entering the house, these may still be released from the interior over an unknown period of time[1, 2].

In the past VI models have been used to gain insight into VI when no field or experimental data has been available. Previously examples of VI modeling studies are the role of rainfall in VI[12], or drivers of temporal variability in some of the aforementioned sites[13]. However, while many VI models include a sorption term in the governing equation for contaminant transport in soils, none have explored the role of sorption in VI in a transient simulation. The reason for this is two-fold. First, there has been a general lack of interest in sorption and VI thus far. Secondly, the vast majority of VI modeling efforts and studies has focused on steady-state analyses of VI, and

sorption only affects soil contaminant transport in time-dependent scenarios.

To bridge this knowledge gap we will begin to explore the role of sorption in VI through a combined effort of experimental and simulation work. Sorption data of TCE on various common indoor materials and Appling soil will be measured in a fixed bed sorption experiment. These sorption data will then be incorporated into a three-dimensional finite element model of VI. For this purpose we will consider a prototypical VI scenario where a free-standing house with a basement is overlying a homogenously contaminated groundwater source. Using this model we will investigate how the dynamic contaminant transport is affected in general by sorption, how indoor sorption materials affect indoor air concentration as the building's pressurization fluctuates and how indoor air concentration are affected by indoor materials following successful mitigation of the structure.

2. Methods

2.1. Experimental Setup

The TCE dynamic sorption process of different building materials were determined by use of a method schematically shown in Figure 1. This method involved a selected material contained in an adsorption column through which TCE-containing gas was passed, and subsequent thermal desorption and measurement of the total amount of adsorption. During the adsorption part of the process, stainless steel tubes were packed with building materials held in place by glass wool. The amount of building material normally held in the tube was around 1 g. It was determined that neither the glass wool nor the stainless steel tube would retain significant amounts of TCE. The sample-containing tubes were first exposed desired low concentrations of TCE in nitrogen, which were then allowed to interact with the flow for varying periods of time. The typical flow rate of the nitrogen was 60 ml/min and the concentrations of TCE was around 1.1 ppbv. All of these adsorption experiments were conducted at room temperature. After a given time of exposure to the TCE-containing flow, that flow was stopped, and the sample tube was attached to a sorbent tube placed downstream of the sample tube. The sample tube was arranged such that the direction of the nitrogen flow in the subsequent desorption process was opposite that of the TCE-containing nitrogen flow during the adsorption process. During the thermal desorption step, the sample containing tube was covered by a heating mantle which permitted its heating at 100 °C. This allowed fully desorbing the TCE which

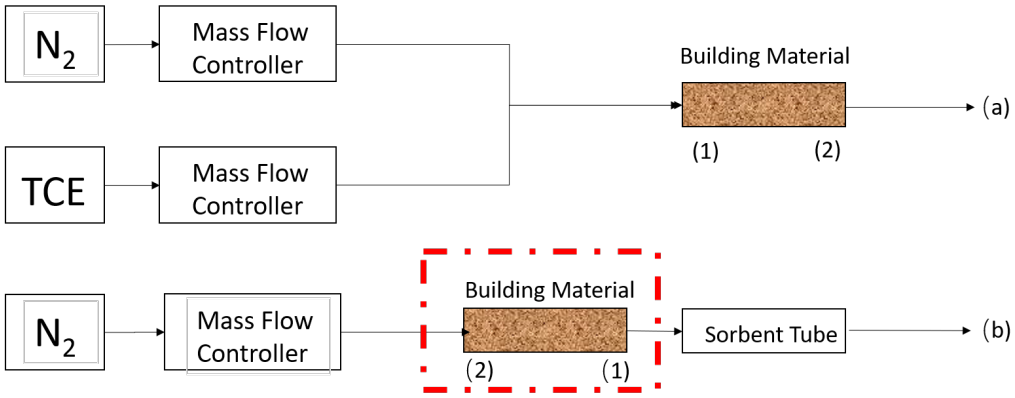

Figure 1: Schematic of experimental setup.

had been held on the sample into a pure nitrogen flow, which carried it to the room temperature downstream sorbent tube, where it was again fully adsorbed. These tubes fully capture all of the TCE desorbed, from the samples, and the amount of TCE was analyzed by Gas Chromatography (GC) with an Electron Capture Detector(ECD).

2.2. Numerical Model

To investigate the role of sorption in VI, we consider a simple VI scenario. Here we consider a house with a 10 by 10 m footprint, with the foundation bottom located 1 m below ground surface (bgs). The sole contaminant source is an uniformly TCE contaminated groundwater located 4 bgs, and the soil surrounding the house is assumed to homogenous and of a singular type. All contaminant vapors are assumed to enter the house through breaches in the foundation, modeled as a 1 cm wide crack that runs along the perimeter of the house. Finally we assume that sorption processes can occur both in the soil matrix and in the indoor environment (on various indoor materials).

Modeling this scenario requires us to simulate a couple of physics, many of which depend and interact with each other. The governing equations and the physics they govern are:

1. van Genuchten retention model - soil moisture.
2. Darcy's Law - air flow in the porous media.
3. Transport equation - contaminant transport in porous media.
4. Continuously stirred tank reactor (CSTR) - contaminant concentration in the indoor environment.

Figure 2: The vapor intrusion model

These physics are implemented in COMSOL Multiphysics, a commercial finite-element method package, which is used to solve our model. It is important to note that the indoor environment is implicitly modeled, but instead only given by the CSTR equation; the soil domain is explicitly modeled.

2.2.1. Vadose Zone Moisture Content

Since the contaminant transport occurs through three-phased the vadose zone, it is important that we correctly account for soil moisture content and its effect on advective and diffusive transport. In this modeled scenario, we assume that the soil moisture is at steady-state and does not change, and thus the soil moisture content is given by the retention model developed by van Genuchten.

The van Genuchten retention model gives the soil water saturation as a function of elevation above groundwater. In turn this gives the water and gas filled porosities, and the relative permeability of the soil matrix.

$$\mathrm{Se} = \begin{cases} \frac{1}{(1+\alpha z^n)^m} & z < 0 \\ 1 & z \geq 0 \end{cases} \tag{1}$$

$$\theta_w = \begin{cases} \theta_r + \mathrm{Se}(\theta_s - \theta_r) & z < 0 \\ \theta_s & z \geq 0 \end{cases} \tag{2}$$

$$k_r = \begin{cases} \mathrm{Se}^l \left[1 - \left(1 - \mathrm{Se}^{\frac{1}{m}}\right)\right]^2 & z < 0 \\ 0 & z \geq 0 \end{cases} \tag{3}$$

Se is the saturation, and ranges from 0 to 1, which represent completely unto fully saturated; z is the elevation above the groundwater in meters; θ_r, θ_s, θ_w, and θ_g are the residual moisture content, saturated porosity (or just porosity), and water and air filled porosities respectively. All units are in volume of phase divided by the volume of soil; k_r is the relative permeability of water, which modifies the saturated permeability. This too ranges from 0 to 1, indicating completely im- and permeable respectively. $1 - k_r$ gives the relative permeability of air.

2.2.2. Gas Flow In The Vadose Zone

The gas flow in the vadose zone is governed by a modified version of Darcy's Law. Originally, Darcy's Law was developed to describe flow in

saturated porous media, but since we're interested in flow in unsaturated media, modification is necessary. An effective permeability that depends on the relative permeability from van Genuchten is introduced to allow for correct flow profiles in unsaturated porous media.

The vapor flow governing equation is given by

$$\frac{\partial}{\partial t}(\rho\theta_s) + \nabla \cdot \rho\Big(- \frac{(1-k_r)\kappa}{\mu}\nabla p\Big) = 0 \tag{4}$$

Here ρ is the fluid density; ∇ is the del operator; κ is the saturated permeability; μ is the fluid viscosity; and p is the fluid pressure. We assume that the contaminant vapors are so dilute that the gas flow properties can be taken to be those of air, and specifically at 20 °C and all the transport properties may be found in Table 1.

Boundary Conditions. To solve (4) we assign the atmosphere boundary (see Figure 2) to be at reference pressure and act as a gauge, i.e. zero pressure. The foundation crack boundary is assigned the indoor-outdoor pressure difference value. Remaining boundaries are no-flow boundary conditions.

Atmosphere	$p = 0$ (Pa)	(5)
Foundation crack	$p = p_{\text{in/out}}$ (Pa)	(6)
All other	$-\vec{n} \cdot \rho_{\text{air}}\vec{u} = 0$ (kg/(m$^2 \cdot$ s))	(7)

Here $\vec{n}$ and $\vec{u}$ are the boundary normal and gas velocity vectors.

Initial Conditions. For steady-state problems, the initial conditions don't matter, but is simply zero for the entire domain. When solving transient, the initial conditions are given by the steady-state solution.

2.2.3. Mass Transport In The Vadose Zone

Contaminants in the vadose zone exist in three phases - gaseous, solved in water, and sorbed onto soil particles. While there are three distinct phases, the water and gas phases are related via Henry's Law (8).

$$c_g = K_H c_w \tag{8}$$

Where c_g and c_w are the gas and water phase concentrations respectively in mol/m^3; K_H is the dimensionless Henry's Law constant.

In this work, we consider sorption between the soil and vapor phases, as a function of the water contaminant concentration, through linear sorption (9).

$$c_s = K_{\text{ads}} \rho_b c_g = K_{\text{ads}} \frac{\rho}{1-\theta_t} K_H c_w \tag{9}$$

Here the c_s is the solid phase concentration in mol/kg; ρ_b is the bulk density of the soil kg/m^3, which is given by the density ρ and the total soil porosity θ_t; K_{ads} is the sorption isotherm in m^3/kg. Using Henry's Law and the linear isotherm we can express the total contaminant concentration in terms of the water contaminant concentration.

Mass transport in the vadose zone is governed by diffusion and advection and is given by (10).

$$R\frac{\partial c}{\partial t} = \nabla \cdot [D_{\text{eff}} \nabla c] - K_H \vec{u} \cdot \nabla c \tag{10}$$

The first term in (10) gives the change in contaminant water concentration with respect to time, modified by the *retardation factor*, R, which is discussed below; The second is the effective diffusive flux which is modified by the effective diffusion coefficient D_{eff} which is also discussed below. The third is the advective flux where $\vec{u}$ is the soil-gas velocity from Darcy's Law, which when multiplied with K_H gives the gas phase concentration advective flux.

Contaminant entry into the building. The contaminant enters the building through a combination of advection and diffusive fluxes and is given by (11).

$$j_{ck} = \begin{cases} u_{ck} c_g - \frac{D_{\text{air}}}{L_{\text{slab}}}(c_{in} - c_g) & u_{ck} \geq 0 \\ u_{ck} c_{in} - \frac{D_{\text{air}}}{L_{\text{slab}}}(c_{in} - c_g) & u_{ck} < 0 \end{cases} \tag{11}$$

Here the j_{ck} is the molar contaminant flux into the building in mol/(m$^2 \cdot$ s); D_{air} is the contaminant diffusion coefficient in pure air in m^2/s; L_{slab} is the thickness of the foundation slab in m. The flux expression changes if there is a bulk flow into the building, i.e. $u_{ck} \geq 0$, or out of the building.

Retardation factor. As the contaminants are transported through the vadose zone, the partitioning between the various phases increases the contaminant residency time, retarding the transport of contaminants. This effect is represented by R which is the retardation factor (12).

$$R = \theta_w + \theta_g K_H + \rho_b K_H K_{\text{ads}} \tag{12}$$

Here θ_w, θ_g are the water and gas filled soil porosities; K_{ads} is the solid-gas phase sorption isotherm in m^3/kg. The diffusive and advective transport retardation is proportional to the inverse of R.

$$D_{\text{retarded}} = \frac{D_{\text{eff}}}{R} \tag{13}$$

$$\vec{u}_{\text{retarded}} = \frac{\vec{u}}{R} \tag{14}$$

It should be noted that the soil-gas velocity, $\vec{u}$, is not retarded in of itself, but rather just the contaminant being transported through advection, giving a effective bulk velocity.

Effective diffusivity. The effective diffusivity in the vadose zone varies with the soil moisture content, from being close to that in water when fully saturated and vice versa. Millington-Quirk developed (15) which describes the effective diffusivity in variably saturated porous media.

$$D_{\text{eff}} = D_{\text{water}} \frac{\theta_w^{\frac{7}{3}}}{\theta_t^2} + \frac{D_{\text{air}}}{K_H} \frac{\theta_g^{\frac{7}{3}}}{\theta_t^2} \tag{15}$$

Where the porosity fractions are the water and gas phase tortuosity terms; D_{air} and D_{water} are the contaminant diffusion coefficient in air and water respectively in m^2/s.

Boundary Conditions. A few boundary conditions are required to solve (10). In this model, the sole contaminant source is assumed to be the homogenously contaminated groundwater, which we assume to have a fixed concentration. The atmosphere acts as a contaminant sink, and any contaminant that makes it to this boundary is ifinitely diluted, thus this is simply a zero concentration boundary condition. Contaminants leave the soil domain and enter the building through a combination of advective and diffusive gas phase transport. The last boundary condition is applied to all other boundaries and is a no-flow boundary.

Groundwater	$c_w = 0 \ (\text{mol}/\text{m}^3)$	(16)
Atmosphere	$c_w = c_{gw} \ (\text{mol}/\text{m}^3)$	(17)
Foundation crack	$-\vec{n} \cdot \vec{N} = -\frac{j_{ck}}{K_H} \ (\text{mol}/(\text{m}^2 \cdot \text{s}))$	(18)
All other	$-\vec{n} \cdot \vec{N} = 0 \ (\text{mol}/(\text{m}^2 \cdot \text{s}))$	(19)

$\vec{n} \cdot \vec{N}$ is the dot product between the boundary normal vector and the contaminant flux; $j_c k$ is the contaminant vapor flux into the building. We assume that only contaminants in the gas phase enter the building, and dividing j_{ck} by K_H we get proper accounting in terms of the water phase concentration.

Initial Conditions. For a steady-state condition the initial conditions don't matter, but are set to be zero everywhere. For transient simulations in this work, the steady-state solution is always used as an initial condition.

2.2.4. Indoor Environment

The indoor air space is modeled as a continuously stirred tank reactor (CSTR) given by (20). Contaminants are assumed to only enter through the foundation crack, represented by n_{ck}, which is calculated by integrating the contaminant flux over the foundation crack boundary. The product of air exchange rate, which govern how many house volumes are exchanged with the outside per time unit, and indoor air contaminant concentration gives the contaminant exit rate. The sorption of contaminant is given by the sorption reaction term in (22) and the sorbed contaminant concentration is given by (21).

$$V_{\text{bldg}} \frac{\partial c_{\text{in}}}{\partial t} = n_{\text{ck}} - A_e c_{\text{in}} V_{\text{bldg}} + r_{\text{sorb}} V_{\text{mat}} \tag{20}$$

$$V_{\text{mat}} \frac{\partial c_{\text{sorb}}}{\partial t} = -r_{\text{sorb}} V_{\text{mat}} \tag{21}$$

$$r_{\text{sorb}} = k_1 c_{\text{sorb}} - k_2 c_{\text{in}} \tag{22}$$

$$n_{\text{ck}} = \int_{A_{ck}} j_{ck} dA \tag{23}$$

Here V_{bldg} and V_{mat} are the indoor control volume and volume of indoor material in m^3; c_{in} and c_{sorb} are the indoor and sorbed (onto the indoor material) contaminant concentrations in mol/m^3; n_{entry} is the contaminant entry rate in mol/s, which is calculated by integrating the contaminant flux j_{ck} over the foundation crack area; r_{sorb} sorption rate in $\text{mol}/(\text{m}^3 \cdot \text{s})$; k_1 and k_2 are desorption and sorption reaction constants in 1/s.

Fitting Kinetic Parameters. To calculate the indoor sorption rate we need k_1 and k_2. These values are found by solving (22) numerically and then finding the best k_1 and k_2 by fitting them to the experimental data via least square.

Table 1: Transport properties and model parameters

We use Runge-Kutta method of order 5(4) as the numerical solve, which is implemented together with the least square method in the SciPy python package[14].

3. Results & Discussion

3.1. Fitting Sorption Parameters

Using the numerical fitting scheme described in section 2.2.4 with the sorption data from the method described in section 2.1, the kinetic sorption parameters k_1 and k_2 are fitted. Figure 3 shows the result of this fitting and the sorption data for three select materials - wood, Appling soil, and cinderblock concrete. The k_1 and k_2 represent the rate at which TCE desorbs and sorbs respectively onto/from the material of interest. The equilibrium sorption constant is, using the formulation in (22), given by

$$K = \frac{k_1}{k_2} \tag{24}$$

and is used as the sorption isotherm. Here a small K indicate that there is a greater propensity for contaminant sorption.

To use the soil sorption isotherm in (10) K needs to be converted from being unitless to m^3/kg. This is done by multiplying the inverse of K isotherm with inverse of the soil bulk density ρ_b, which is taken to be $1460\ \mathrm{kg}/\mathrm{m}^3$.

$$K_{\text{ads}} = \frac{1}{K\rho_b} = 5.28\ (\mathrm{m}^3/\mathrm{kg}) \tag{25}$$

Table 2 shows the fitted parameters for the tested materials. Based on this these results we can see that cinderblock and soil have orders of magnitude larger sorption capacities than wood or drywall does. We can also see by the k_2 values that soil and cinderblock sorb quickly, much faster than a material with similar sorptive capacity such as paper.

3.2. Soil Sorption's Retarding Effect

Building pressurization is a key factor in VI that influences the advective contaminant transport. The magnitude of change in response to a pressurization change is significantly influenced by a range of factors, such as soil

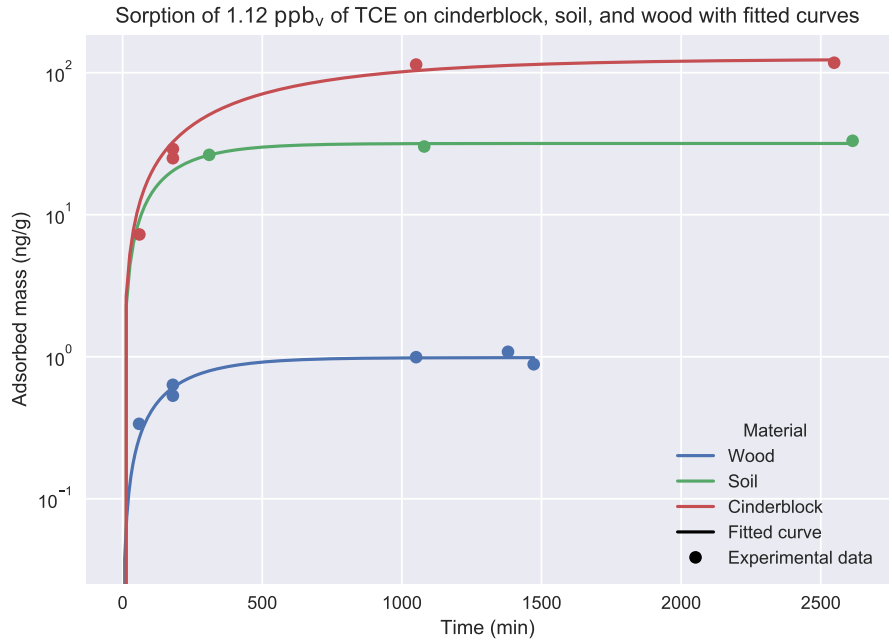

Figure 3: Experimental data of sorption of TCE onto three select materials as well as fitted sorption rates based on the kinetic model (22).

Table 2: Fitted kinetic sorption parameters based on sorption experiment data.

Material	k_1 (1/hr)	k_2 (1/hr)	K
Wood	0.32	44.90	$7.10 \cdot 10^{-3}$
Drywall	0.41	87.94	$4.65 \cdot 10^{-3}$
Carpet	0.26	58.74	$4.42 \cdot 10^{-3}$
Paper	0.04	88.37	$4.55 \cdot 10^{-4}$
Soil	0.34	2636.57	$1.30 \cdot 10^{-4}$
Cinderblock	0.10	4175.16	$2.40 \cdot 10^{-5}$

permeability, foundation depth, or soil moisture. To demonstrate the effect that soil sorption has on contaminant soil mass transport in the VI context, we run two types transient simulation where initially the modeled structure is at a steady -5 Pa, i.e. slightly depressurized. At the start of the simulation, the building building is 1) further depressurized to -15 Pa, or 2)

overpressurized to 15 Pa, and the simulation is allowed to run for 72 hours.

$$\text{Depressurization}: \ \Delta p_{\text{in/out}} = \begin{cases} -5, & t = 0 \text{ (hr)} \\ -15, & 0 < t \leq 72 \text{ (hr)} \end{cases} \tag{26}$$

$$\text{Overpressurzation}: \ \Delta p_{\text{in/out}} = \begin{cases} -5, & t = 0 \text{ (hr)} \\ 15, & 0 < t \leq 72 \text{ (hr)} \end{cases} \tag{27}$$

For each of these cases, the simulation is run using two different soil types - sand and sandy loam. Sand is assumed here to not sorb any TCE, while for sandy loam a range of sorption isotherms are used. These range from no sorption ($K_{\text{ads}} = 0$ (m^3/kg)) to the experimentally determined sorption isotherm ($K_{\text{ads}} = 5.28$ (m^3/kg)) in intervals multiplicative by 10^{-2}. With the experimentally determined isotherm, we see that the ratio between sorbed concentration and soil-gas phase concentration is 7708, i.e. there is a much larger amount of sorbed contaminant. When $K_{\text{ads}} = 5.28 \cdot 10^{-4}$ (m^3/kg) this ratio is roughly unity (0.77), which is good to keep in mind in the following discussion. These ranges of values can be used both to represent a soil that has a smaller sorptive capacity or a situation where the sorbed and gas phase has not quite reached equilibrium.

In the top panel of Figure 4, the indoor air contaminant concentration as the simulated building is undergoing the pressurization in (26) case. Here we can see that for the case when the surrounding soil consists of sand, the indoor concentration increases rapidly as the building is further pressurized. The rate of increase decreases significantly for the sandy loam cases, and progressively retards are the sorbed mass increases (K_{ads} increases).

The bottom left panel shows how far away the indoor air concentration (as attentuation factor) for each case is from reaching equilibrium. At the start of the simulation, the building starts with an attenuation of α_0, which is the steady-state concentration when the building is pressurized with -5 Pa. As the building is further depressurized to -15 Pa, the indoor air concentration will approach a new equilibrium state α_{eq} (the result of which is from a steady-state simulation at that pressurization). By plotting $\frac{|\alpha - \alpha_0|}{|\alpha_{eq} - \alpha_0|}$ we can easily see how far away we are from the new equilibrium state, and a value of 0 represents that we are at the initial concentration, i.e. $\alpha = \alpha_0$, and a value of 1 represents $\alpha = \alpha_{eq}$.

This sort of analysis is applied to the bottom right panel as well, but instead of the indoor air concentration (as attentuation factor), we consider

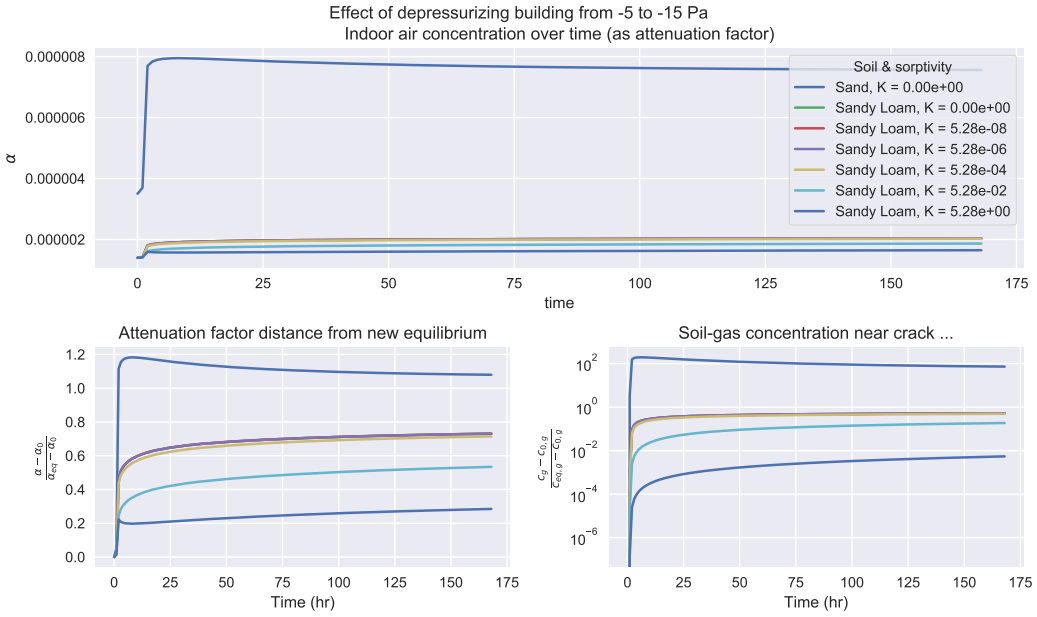

Figure 4

the average soil-gas concentration in a 5 cm diameter cylinder that envelop the entire perimeter crack. The choice of 5 cm is arbitrary, but helps illustrate what happens with the near-foundation-crack soil-gas concentration, changes in which allow us to better understand how the contaminant is transported into the building from the soil. The same could be done for the soil-gas velocity of course, but the rate of soil-gas velocity change is virtually the same for all of these cases, and reaches the new equilibrium velocity very quickly (much faster than the concentration) and is thus omitted from the figure.

Before discussing the role of sorption here, we can first compare the non-sorbing sand and sandy loam cases. Due to the higher permeability and lower moisture content, sand is significantly more permeable to gas flow than sandy loam (see Table 1 for permeability values). Consequently the advective transport through the foundation crack is much more significant, which is indicated by a Péclet number of around 4 versus 0.2 at a -15 Pa pressurization for sand and sandy loam respectively.

Due to the advection dominated transport mechanism in the sand case, the indoor air concentrations are temporarily elevated above the equilibrium

concentration at -15 Pa, while the soil-gas concentration moves further away from equilibrium. (Note that the absolute distance from equilibrium is plotted in Figure 4 which is why at first glance one might think that the soil-gas concentration is two order of magnitude higher initially, but actually is two order of magnitude lower.) This phenomena occurs because initially more contaminants are drawn into the building from the near crack area than can be resupplied, temporarily depleting the local soil-gas contaminant concentration.

One can notice that many of the sandy loam lines overlap, and start diverging from each other when $K_{\text{ads}} = 5.28 \cdot 10^{-4}$ (m^3/kg), at the point where the ratio of sorbed and soil-gas concentration are roughly equal. We see that this divergence occurs simultaneously in the indoor air and soil-gas contaminant concentration. However, since the indoor air concentration depend on the soil-gas concentration, we know that this is where the relevant difference is.

The simple reason for this is that it is at this threshold the sorptive contribution to the retardation factor (12) starts to becomes larger than the other terms.

$$\rho_b K_H K_{\text{ads}} > \theta_w + \theta_g K_H \tag{28}$$

Thus it is at this point that the contaminant transport in the soil starts to become retarded by sorption. The physical reason for this is that the partitioning between the various phases gives a residence time as the contaminant is transported. Under VI conditions, the values of $\theta_w + \theta_g K_H$ are bounded to relatively small values, while K_{ads} can vary by orders of magnitude, making sorption potentially a very significant retarder for soil transport.

Figure 5 shows the same sort of analysis as in Figure 4 but with the building pressurization following (27). The results here are more or less the same, with the notable exception that in the sand case, the final equilibrium concentration is not initially exceeded. As the building is overpressurized, the indoor contaminant are pushed out into the soil. Since the indoor air concentration is lower than the soil-gas concentration, this is entirely expected.

3.3. Indoor Material Sorption And Dynamics

We have now explored the effect that sorption has on contaminant mass transport in the sub-surface soil and seen its retarding effect. Now we turn to exploring the effect of sorption onto/from various indoor materials has on the indoor air contaminant concentration. (Here we assume that there is no soil sorption.)

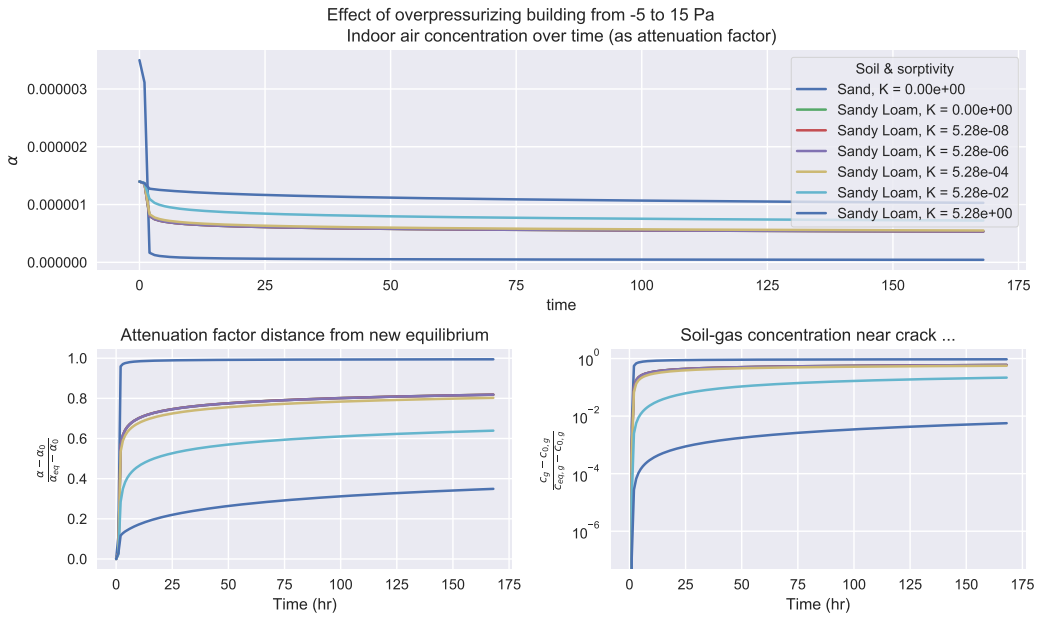

Figure 5

To study this we consider the basement (the indoor air space) and assume that the inside surfaces are entirely made up of one of the materials we studied in 3.1. We also assume that the material covering the indoor surfaces has a certain thickness or depth that the contaminants can penetrate - giving a certain volume or mass of sorbing material in the indoor. Table 3 shows the surface area, penetration depth, and volume of each material studied. While obviously some of these rooms are non-conventional and arbitrarily designed, i.e. you're unlikely to find a room with carpeted walls, floors, and ceiling, they do present some limiting cases of the potential effect of sorption onto/from these materials.

The modeled building then undergoes a pressurization cycle, where at start of the simulation it is depressurized at -5 Pa and at steady-state. The building is then sequentially depressurized to -15 Pa, then pressurized to 15 Pa, and finally again depressurized to -5 Pa. For each sequence, the new pressurization is maintained for 24 hours. This pressurization cycle may be seen in the top left panel of 6. The choice of pressurization cycle is somewhat arbitrary, but ours can be used to represent limiting cases of natural pressurization variation, or artificially induced pressurization. Figure

Material	d_{p} (mm)	V_{mat} (m^3)
Cinderblock	5	1.6
Wood	1	0.32
Drywall	10	3.2
Carpet	10	3.2
Paper	0.1	0.032

Table 3: The assumed contaminant penetration depth and subsequent volume of the sorbing indoor materials. The material surface area is assumed to be the same, and each material completely cover the surfaces of a 10x10x3 meter room.

6 shows the result of these simulations.

The change in indoor air contaminant concentration over this pressurization cycle is shown in the bottom panel of Figure 6. First we consider the reference case - where there is no sorbing indoor materials present. (The blue line is the reference case, which may be difficult to see as the wood and carpet lines overlap.) Here we see that as the building is depressurized, the indoor air contaminant concentration increases quickly in response to the pressurization change, and is approaching an equilibrium.

By observation we can see that the presence of the various studied building materials in the indoor environment has a very different effect on the change in indoor air contaminant concentration. The presence of wood and carpet has close to no effect on the indoor air concentration. While cinderblock has a very significant effect, preventing almost any change in indoor concentration. Drywall and carpet is in the middle significantly delays the rate of change in the indoor concentration, but for each 24 hour cycle, roughly the same indoor concentration is reached as the reference case.

The disparity of these result is explained by the the top right panel of Figure 6. Here the de- and sorption rates in μg/hr for each considered indoor material is shown. A positive and negative value here indicate that contaminant is desorbed respectively sorbed to and from the material. To understand this figure, it is useful to refer back to Table 2 which show the sorption and desorption rate constant k_1 and k_2 respectively, and the sorption equilibrium constant K (a smaller value indicate a larger sorptive capacity).

First we consider to the depressurization part of the cycle (1-25 hours). (Here see that the reference case has no sorption at all, by definition.) And similar to the indoor concentration panel, we see that the wood, drywall,

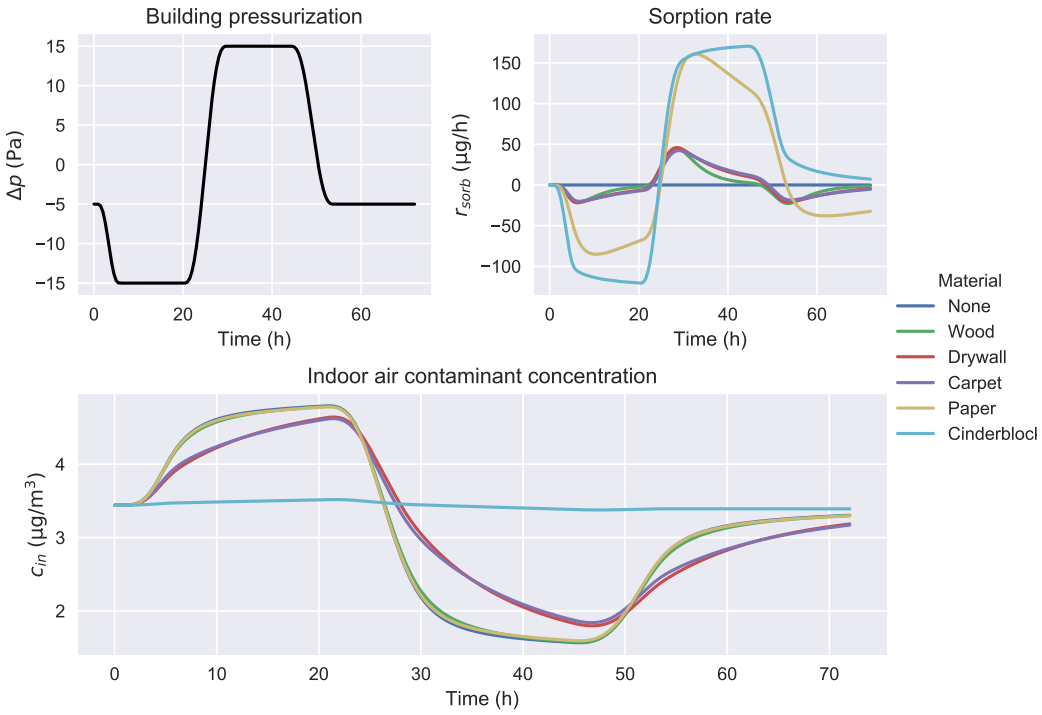

Figure 6: Comparison of how sorption onto/from various indoor materials affect the indoor air contaminant concentration (bottom) of a building that undergoes a pressurization cycle (top left). The rate of de- and sorption for each considered material during the cycle are also shown (top right) and is governed by (22).

and carpet cases overlap. This is explained by these materials have similar sorptive capacities (K) and sorptive rates (k_2). Paper by contrast has a similar shape to the three previously mentioned, while the magnitude is significantly larger. This is because the K value for paper is one order of magnitude larger, indicating that wood, drywall, and carpet saturate with contaminant vapors over the time period, while paper does not. Cinderblock has a further order of magnitude larger K value, thus is even further away from being saturated, which explains the even faster sorption rate.

Next we consider the overpressurzation period (25-49 hours). Again we see here that wood, drywall, and carpet behave the similarly for the same reasons as before, i.e. the desorption rate constants k_1 and sorption equilibrium constants K are similar. This means that these reach the new sorbed contaminant saturation at roughly the same time.

Here it is important to note that due to the diffusion dominated transport

through the foundation crack, even though the building is overpressurized, there is substantial contaminant entry. And because the sole contaminant source is the modeled contaminated groundwater, the sorbed equilibrium is relative to this entry rate.

Paper and cinderblock initially behave very similarly during the overpressurization period and desorb contaminants quickly. However, paper reaches its saturation limit after a relatively short time, while cinderblock has not even at the end of the overpressurization cycle. Since the desorption rate constants k_2 are relatively similar for the materials, thus this disparity is primarily due to the different sorption equilibrium constants K.

Lastly, we consider the final period where the pressurization goes back to its initial state (49-72 hrs). Here we see that the reference case does not quite return to the initial indoor concentration. Thus the contaminant entry rate has not equilibrated yet, due to the soil contaminant concentration has not done so either. Like in the previous analysis we again see that the wood, drywall, and carpet cases don't differ from the reference. The paper case is slightly more different, but for the same reasons that have already been discused. Cinderblock is unique here though, as we clearly see that it is releasing contaminants, due to the previous change in contaminant concentration has been so significantly retarded.

From this simulation work we can see how varied the effect of sorbing indoor materials are. Most of the tested materials only have a moderate effect on the indoor air contaminant concentration dynamics, with the notable exception of cinderblock, which effectively enforces as pseudo-steady-state. However we also see from the analysis of the sorption dynamics that the de- and sorption rate constants k_1 and k_2 are less important than the sorptive capacity K of the material.

3.4. Indoor Material Sorption And Mitigation

The work done by us and others have shown the large sorptive capacities of various common materials. The desorption of the sorbed contaminants may have significant impact on the efficacy of various mitigation systems. To investigate this we turn to our model and consider a scenario where initially the modeled building is depressurized with -5 Pa and at the start of the simulation some perfect mitigation scheme is turned on and the contaminant entry n_{entry} in (**??**) goes to zero. We also assume that for each case, the indoor environment contains the same amount of indoor material as described in

section 3.3. The air exchange rate is assumed to remain a constant 0.5 per hour for the entire 72 hour simulation time.

The decrease in indoor air concentration (as attenuation factor α) for each simulated case is seen in Figure 7. As excepted, when there is no sorbing indoor materials, i.e. our reference case, the indoor concentration decreases log-linearily. We can also see that the contaminant desorption from the materials maintain a higher indoor air concentration relative to reference, with cinderblock again shown to have the great impact.

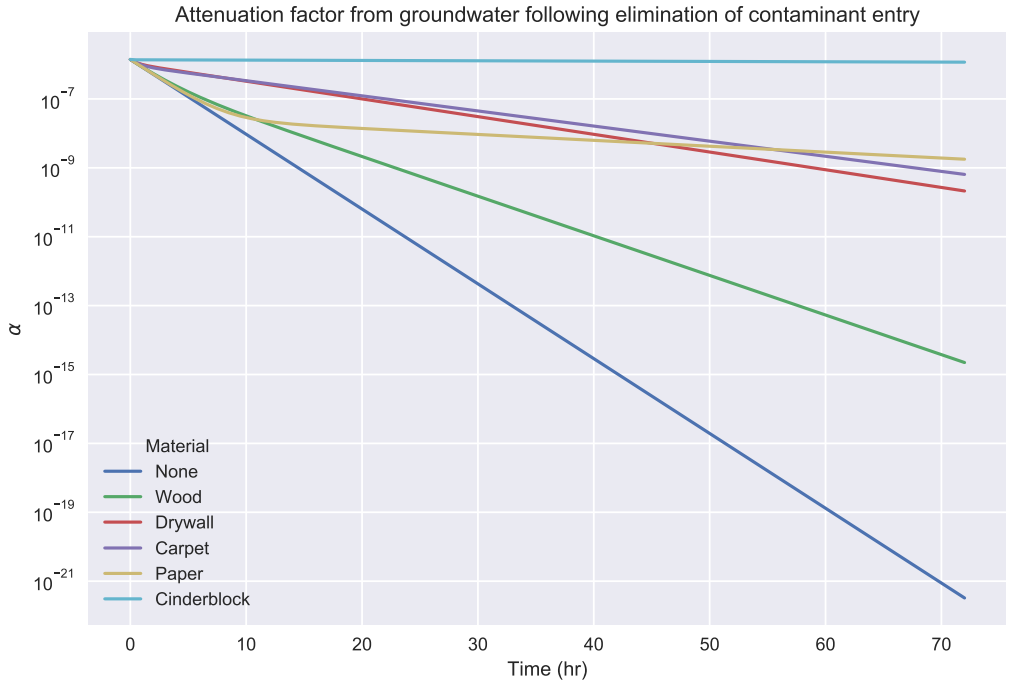

Figure 7

4. Conclusions

Acknowledgements

This project was supported by grant ES-201502 from the Strategic Environmental Research and Development Program and Environmental Security Technology Certification Program (SERDP-ESTCP).

Declaration of interest: none

References

[1] R. Meininghaus, L. Gunnarsen, H. N. Knudsen, Diffusion and Sorption of Volatile Organic Compounds in Building Materials-Impact on Indoor Air Quality, Environ. Sci. Technol. 34 (15) (2000) 3101–3108. doi:10.1021/es991291i.

[2] R. Meininghaus, E. Uhde, Diffusion studies of VOC mixtures in a building material, Indoor Air 12 (4) (2002) 215–222. doi:10.1034/j.1600-0668.2002.01131.x.

[3] F. D. Tillman, J. W. Weaver, Review of Recent Research on Vapor Intrusion (2005) 47.

[4] X. Wang, Y. Zhang, J. Xiong, Correlation between the solid/air partition coefficient and liquid molar volume for VOCs in building materials, Atmospheric Environment 42 (33) (2008) 7768–7774. doi:10.1016/j.atmosenv.2008.05.030.

[5] J. Xu, J. S. Zhang, X. Liu, Z. Gao, Determination of partition and diffusion coefficients of formaldehyde in selected building materials and impact of relative humidity, J. Air Waste Manag. Assoc. 62 (6) (2012) 671–679. doi:10.1080/10962247.2012.665812.

[6] A. Bodalal, J. S. Zhang, E. G. Plett, A method for measuring internal diffusion and equilibrium partition coefficients of volatile organic compounds for building materials, Building and Environment 35 (2) (2000) 101–110. doi:10.1016/S0360-1323(99)00005-0.

[7] U.S. Environmental Protection Agency, OSWER Technical Guide for Assessing and Mitigating the Vapor Intrusion Pathway From Subsurface Vapor Sources To Indoor Air (2015).

[8] C. Holton, Y. Guo, H. Luo, P. Dahlen, K. Gorder, E. Dettenmaier, P. C. Johnson, Long-Term Evaluation of the Controlled Pressure Method for Assessment of the Vapor Intrusion Pathway, Environ. Sci. Technol. 49 (4) (2015) 2091–2098. doi:10/f64j45.

[9] C. C. Lutes, R. S. Truesdale, B. W. Cosky, J. H. Zimmerman, B. A. Schumacher, Comparing Vapor Intrusion Mitigation System

Performance for VOCs and Radon, Remediation 25 (4) (2015) 7–26. doi:10/gd6dfn.

[10] U.S. Environmental Protection Agency, Assessment of Mitigation Systems on Vapor Intrusion: Temporal Trends, Attenuation Factors, and Contaminant Migration Routes under Mitigated And Non-mitigated Conditions (2015).

[11] T. McHugh, P. Loll, B. Eklund, Recent advances in vapor intrusion site investigations, Journal of Environmental Management 204 (2017) 783–792. doi:10/gd6dgk.

[12] R. Shen, K. G. Pennell, E. M. Suuberg, A numerical investigation of vapor intrusion — The dynamic response of contaminant vapors to rainfall events, Science of The Total Environment 437 (2012) 110–120. doi:10/f4fp9s.

[13] J. G. V. Ström, Y. Guo, Y. Yao, E. M. Suuberg, Factors affecting temporal variations in vapor intrusion-induced indoor air contaminant concentrations, Building and Environment 161 (2019) 106196. doi:10.1016/j.buildenv.2019.106196.

[14] E. Jones, T. Oliphant, Pearu Peterson, SciPy: Open source scientific tools for Python (2011).